Design, Modeling and Control of a Reaction Wheel Balanced Inverted Pendulum

Conference Paper · June 2018

DOI: 10.1109/ARGENCON.2018.8646093

2 authors:

Gonzalo Belascuen
Instituto Tecnológico de Buenos Aires
1 PUBLICATION **11** CITATIONS
SEE PROFILE

Nahuel Aguilar
Instituto Tecnológico de Buenos Aires
1 PUBLICATION **11** CITATIONS
SEE PROFILE

Design, Modeling and Control of a Reaction Wheel Balanced Inverted Pendulum

Gonzalo Belascuen[†1] and Nahuel Aguilar[†2]

Department of Mechanical Engineering[†1] and Electrical Engineering[†2], Instituto Tecnológico de Buenos Aires (ITBA)
Av. Eduardo Madero 399, CABA, Buenos Aires, Argentina
[1]gbelascu@itba.edu.ar
[2]naguilar@itba.edu.ar

***Abstract*—This paper presents the mechatronics design, modeling, simulation, implementation and control of an inverted pendulum by applying controlled torques to a reaction wheel. We present a method for finding an optimal mechanical design of the pendulum and reaction wheel for a given electric motor and wheel diameter that maximizes the recovery angle. This paper also describes which parameters to look for during the electric motor selection as well as a method for simulating and comparing the performance of different motors. Finally the real system implementation is described and its performance is compared with simulation. The final design is 34 centimeters tall and can stabilize after being released from an angle of 26 degrees from the vertical. This work was carried out within an undergraduate course on Digital Control Systems at Instituto Tecnológico de Buenos Aires.**

***Resumen*— Este trabajo presenta el diseño mecatrónico, modelado, simulación, implementación y control de un péndulo invertido balanceado con una rueda de inercia. Se presenta un método para encontrar un diseño mecánico óptimo de la rueda de inercia para un dado motor eléctrico y diámetro de la rueda que maximiza la estabilidad contra disturbios externos. Este trabajo también describe qué parámetros son de importancia a la hora de seleccionar un motor y provee un método para comparar diferentes motores. La implementación del sistema real es descripta y finalmente se compara el desempeño del sistema real con el simulado. El diseño final mide 34 centimetros de alto y puede estabilizarse después de ser liberado de un ángulo de 26 grados con respecto a la vertical. Este trabajo fue realizado durante un curso de grado de Control Discreto en el Instituto Tecnológico de Buenos Aires.**

I. Introduction

The reaction wheel balanced inverted pendulum problem has been solved by many authors using several different methods ([1], [2], [3], [4]).

This paper analyses the mechatronic design of such a system by identifying how the parameters affect the control system performance and present methods for finding optimal solutions for this problem. The system performance is quantified by finding the maximum angle from which the pendulum can stabilize after being released with the wheel at rest. This is the parameter that is being optimized on this paper.

A video of the system in action can be found at [5].

4 methods to optimize this parameter are presented. The first method analyzes how different pendulum heights affect the system performance. The second method analyzes how to find the optimal dimensions of the reaction wheel for a given electric motor. The third method identifies the optimal motor reduction coefficient. The fourth method is for comparing different motor options and finding the most suitable for the application.

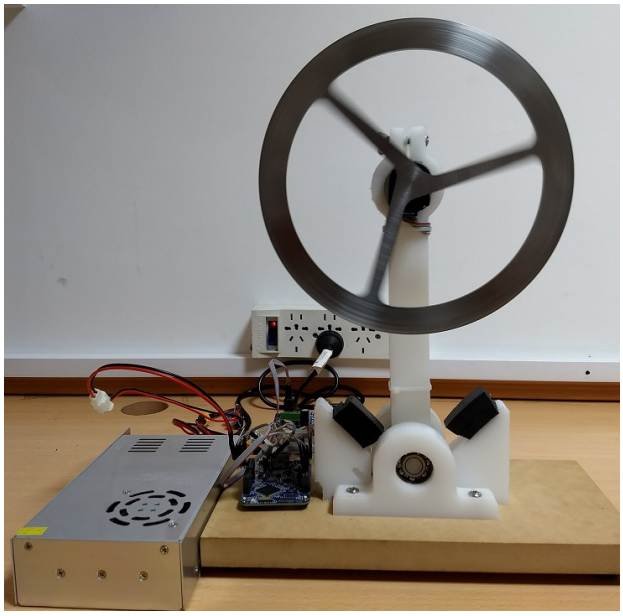

Fig. 1. Implemented System. Front View

Fig. 2. Implemented System. Side View

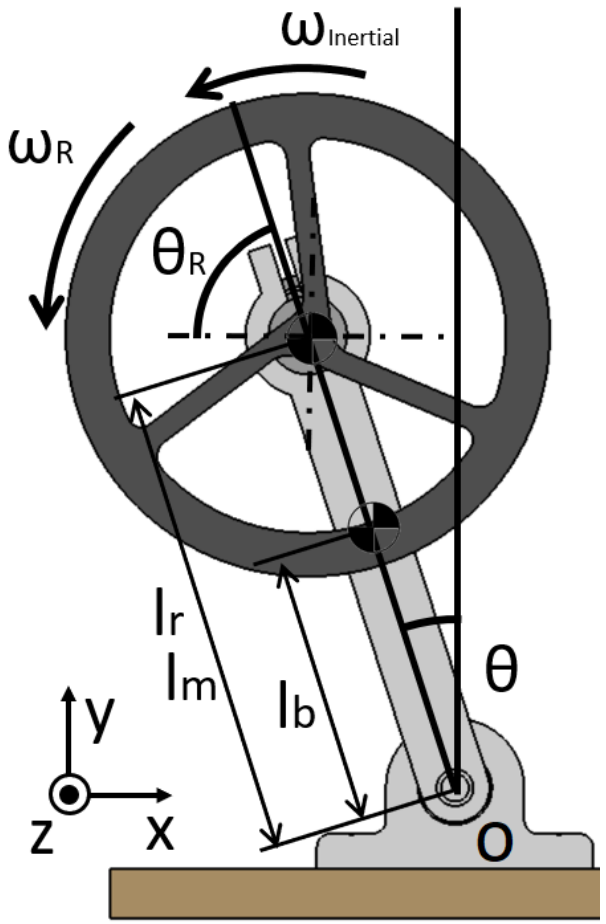

Fig. 3. Coordinate system and name convention definition.

II. System Modeling

A. Notation

- M_m : Motor Mass.
- M_R : Reaction Wheel Mass.
- M_b : Pendulum Arm Mass.
- b_b : Pendulum Arm axis viscous friction.
- l_b : Pendulum Arm center of mass distance to axis.
- l_m : Motor center of mass distance to axis.
- l_R : Reaction wheel center of mass distance to axis.
- g : Gravitational acceleration.
- τ_c : Effective Motor Control torque.

Inertia:

- I_{bo} : Pendulum with respect to point o.
- I_{ro} : Reaction wheel with respect to point o.
- I_{mo} : Motor with respect to point o.
- I_R : Reaction wheel with respect to its center of mass.

Angular Speed:

- ω_R : wheel speed with respect to pendulum arm.
- $\omega_{Inertial}$: wheel inertial speed.

B. Non-linear Model

Fig. 1 and Fig. 2 show the implemented system. Fig. 3 shows the coordinate system definition used to model the system. To model the dynamics of the system, distances, velocities and accelerations must expressed with respect to an inertial frame. The equation of motion of the pendulum is:

$$I_{so}\ \ddot{\theta} = k_{mgl} \cdot \sin\theta - b_b \cdot \dot{\theta} - \tau_c \tag{1}$$

where:

$$I_{so} = I_{bo} + I_{ro} + I_{mo} \tag{2}$$

$$k_{mgl} = (M_b \cdot l_b + M_m \cdot l_m + M_R \cdot l_R) \cdot g \tag{3}$$

and

$$I_{ro} = M_R \cdot l_R^2 \tag{4}$$

$$I_{mo} = M_m \cdot l_m^2 \tag{5}$$

with I_{so} being the total inertia of the pendulum and k_{mgl} being the mass-gravity-length constant. The equation of motion of the reaction wheel is:

$$I_R \cdot \dot{\omega}_{Inertial} = \tau_c \tag{6}$$

It should be noted that for equation (6) the inertial angular velocity $\omega_{Intertial}$ will not be directly measured. Instead, the relative velocity between the reaction wheel and the pendulum arm ω_R will be. The relation between these velocities is:

$$\omega_{Inertial} = \dot{\theta} + \omega_R \tag{7}$$

The reaction wheel and the pendulum arm will accelerate due to the effective motor control torque τ_c. This torque is given by the following equations that model the electric motor:

$$\begin{cases} \tau_c = \tau_e - b_R \cdot \omega_R - \tau_{fd} \cdot \mathbf{sgn}(\omega_R)\ if\ |\omega_R| > 0 & \text{(8a)} \\ \tau_c = 0 \quad if \quad \omega_R = 0 \quad and \quad \tau_e < \tau_{fe} & \text{(8b)} \end{cases}$$

where:

- τ_e : Electric torque
- b_R : Motor viscous friction coefficient
- τ_{fd} : Dynamic friction torque
- τ_{fe} : Static friction torque
- **sgn**() : sign function

Lastly the electric torque is given by the electromechanical model of the motor:

$$\begin{cases} \tau_e = k_t \cdot i & \text{(9a)} \\ R \cdot i + L \cdot \dfrac{\mathrm{d}i}{\mathrm{d}t} = u(t) - k_e \cdot \omega_R & \text{(9b)} \end{cases}$$

where:

- R : Motor coil resistance
- L : Motor coil inductance
- k_t : Motor Torque constant
- k_e : Motor EMF constant
- $u(t)$: Motor terminal voltage

C. Model Linearization

The system is linearized around the steady state point:

$$\begin{cases} \theta^* = 0 & \text{(10a)} \\ \omega_R^* = 0 & \text{(10b)} \end{cases}$$

In equation (1), $\sin\theta$ is linearized around θ^* as θ. No deviation variables need to be defined because the linearization point is at $\theta = 0$.

To linearize equations (8a) and (8b) around $\omega_R = 0$, the dynamic and static frictions cannot be linearized and are therefore ignored. This can be done because they do not have a significant effect on the dynamics of the system.

The linearized system of equations that model the system are:

$$\begin{cases} I_{so} \cdot \ddot{\theta} = k_{mgl} \cdot \theta - b_b \cdot \dot{\theta} - \tau_c & (11) \\ I_R \cdot \dot{\omega}_{Inertial} = \tau_c & (12) \\ \tau_c = \tau_e - b_R \cdot \omega_R & (13) \\ \tau_e = k_t \cdot i & (14) \\ R \cdot i + L \cdot \dfrac{\mathrm{d}i}{\mathrm{d}t} = u(t) - k_e \cdot \omega_R & (15) \\ \omega_R = \omega_{Inertial} - \dot{\theta} & (16) \end{cases}$$

D. State Space Representation

The number of state variables for a system is equal to the number of independent energy storage elements in the system. For this reaction wheel inverted pendulum, four energy storage elements can be identified:

1) Gravitational potential energy of the system.
2) Angular kinetic energy of the system.
3) Angular kinetic energy of the reaction wheel.
4) Magnetic energy stored in the coils of the motor.

The state variables that correspond to these energy storage elements are:

1) θ: Angular position of the pendulum.
2) $\dot{\theta}$: Angular velocity of the pendulum.
3) ω_R: Angular velocity of the reaction wheel.
4) i: Electric current through the motor respectively.

The current can be ignored because the time constant of the RL circuit of the electric motor is very small compared to the mechanical time constants of the rest of the system. Setting $L = 0$ approximates this time constant from very small to zero and therefore eliminating the current as another state variable. The state variables of the system are:

$$x_1 = \theta \quad (17)$$

$$x_2 = \dot{\theta} \quad (18)$$

$$x_3 = \omega_R \quad (19)$$

Relative angular velocity ω_R is defined as a state variable instead of $\omega_{Inercial}$ because, as mentioned before, the encoder mounted on the pendulum will be measuring the relative angular velocity ω_R.

Because of the definition of the state variables, the dynamic equation of the first state is:

$$\dot{x}_1 = x_2 \quad (20)$$

By combining equations (13), (14), (15) and substituting ω_R for x_3, we have:

$$\tau_c = \frac{k_t}{R}u(t) - (\frac{k_t}{R}k_e + b_R)x_3 \quad (21)$$

The dynamic equation of the second state is given by equation (11). Substituting equation (21) we have:

$$\dot{x}_2 = \frac{k_{mgl}}{I_{so}}x_1 - \frac{b_b}{I_{so}}x_2 + \frac{(\frac{k_t}{R}k_e + b_R)}{I_{so}}x_3 - \frac{k_t}{RI_{so}}u(t) \quad (22)$$

The dynamic equation of the third state can be found by taking equation (12) and replacing both the derivative of equation (16) and equation (21) we have:

$$I_R(\dot{\omega}_R + \ddot{\theta}) = \frac{k_t}{R}u(t) - (\frac{k_t}{R}k_e + b_R)x_3 \quad (23)$$

Then taking equation (23), substituting $\dot{\omega}_R$ for $\dot{x}_3$ and $\ddot{\theta}$ for $\dot{x}_2$, then substituting $\dot{x}_2$ for equation (22) and finally isolating $\dot{x}_3$ we obtain:

$$\dot{x}_3 = -\frac{k_{mgl}}{I_{so}}x_1 + \frac{b_b}{I_{so}}x_2 - \frac{I_{so}+I_R}{I_{so}I_R}(b_R + \frac{k_e k_t}{R})x_3 + \dots \\ \dots + \frac{I_{so}+I_R}{I_{so}I_R}\frac{k_t}{R}u(t) \quad (24)$$

Lastly we can express the state space equations in the following matrix form:

$$\dot{X} = AX + Bu(t) \quad (25)$$

$$y = CX + Du(t) \quad (26)$$

with the matrices being:

$$A = \begin{bmatrix} 0 & 1 & 0 \\ \frac{k_{mgl}}{I_{so}} & -\frac{b_b}{I_{so}} & \frac{k_t k_e}{RI_{so}} + \frac{b_R}{I_{so}} \\ -\frac{k_{mgl}}{I_{so}} & \frac{b_b}{I_{so}} & -\frac{I_{so}+I_R}{I_{so}I_R}(b_R + \frac{k_e k_t}{R}) \end{bmatrix} \quad (27)$$

$$B = \begin{bmatrix} 0 \\ -\frac{k_t}{RI_{so}} \\ \frac{I_{so}+I_R}{I_{so}I_R}\frac{k_t}{R} \end{bmatrix} \quad (28)$$

Because all the state variables will be measured, we have:

$$C = \begin{bmatrix} 1 & 0 & 0 \\ 0 & 1 & 0 \\ 0 & 0 & 1 \end{bmatrix} \quad (29)$$

$$D = [0] \quad (30)$$

III. Simulation

Both linear and non-linear simulations of the system were implemented on *MATLAB Simulink* [6]. The linear simulation was used to run batch simulations in a time efficient manner for system optimization. The non-linear simulation was mainly used to validate the predictions of the linear simulation and to compare the performance with the real system.

IV. System Performance evaluation criteria

It's clear that for a given reaction wheel inverted pendulum, the control authority that the motor has over the system depends on the motor characteristics, the dimensions of the pendulum arm and the dimensions of the reaction wheel.

This control authority can be quantified by finding the recovery angle of the system, which is the maximum angle from which the pendulum can become upright by applying full voltage on the motor after being released with no velocity on the reaction wheel.

To find the recovery angle of a given pendulum, a binary search algorithm is performed starting with an initial angle and applying the following conditions:

- If the pendulum cannot stabilize, then the angle is too high decrease angle.
- If the pendulum can stabilize, then the angle is too low increase angle.

We also refer to control authority as system performance.

V. Mechanical Design

The mechanical design of the pendulum arm and reaction wheel aims to maximize the system performance while being simple to manufacture and assemble. The general design procedure of each part consists of:

1) Defining the general geometry of the part with ease of manufacturing and assembly in mind.
2) Parametrize the model of the system.
3) Identify which parameters have the greatest impact on the recovery angle.
4) Make an educated guess on how varying these parameters will affect system performance by looking at the form of the equations.
5) Performing batch simulations of the system sweeping through different values and generating plots.
6) Analyze the plot and determine the optimal value, if any.

The mechanical design is an iterative process including the motor selection. This section will describe the design methodologies used to design each part. The parameter sweep plots presented in this section were performed on the final mechanical design of the system to show the effect that varying these parameters have on the recovery angle. However, because at the time of mechanical design the electric motor was unavailable, these simulations use an estimated model of the electric motor, yielding slightly different recovery angle values than in Sections VIII, IX, X which use a model of the characterized motor. Table I shows the values of the principal dimensions for the final design.

TABLE I
Model Parameters

Parameter	Value	Unit
l_r	207	mm
b_p	20	mm
a_p	30	mm
R_r	105	mm
a_r	10	mm
b	5	mm
t	19	mm
k_e	0.4105	Vs
k_t	0.3568	$\frac{Nm}{A}$
R	2.5	Ω

A. Pendulum Arm Design

Fig. 4 show the general dimensions of the pendulum arm. The lower part attaches to a rotating shaft and the upper part holds the electric motor. Dimensions ap and bp are chosen for ease of manufacture and to provide stiffness to the arm, the effect of varying these dimensions on the system performance is very small.

However the length of the pendulum l_r does have a significant impact on the recovery angle. We can understand this qualitatively by analyzing the sum of forces at an instant in time where the pendulum is at an angle θ, the wheel has no angular velocity and the motor is generating its maximum torque τ_{max}. From equation (1), the condition that makes $\ddot{\theta}$ negative, and therefore accelerating towards the stable position, is:

$$\tau_{max} \geq k_{mgl} \cdot \sin\theta \tag{31}$$

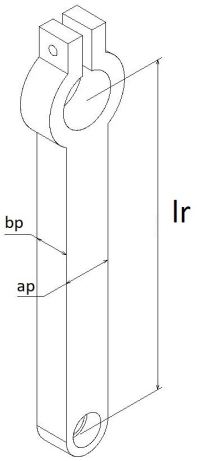

Fig. 4. Pendulum arm general dimensions.

therefore the maximum angle that makes $\ddot{\theta}$ negative is

$$\theta_{max} = \sin^{-1}(\frac{\tau_{max}}{k_{mgl}}) \tag{32}$$

for angles from 0 to $\frac{\pi}{2}$, $\sin^{-1}()$ is an increasing function and therefore to increase θ_{max}, we need to decrease k_{mgl}. From the definition of k_{mgl}, considering that l_R, l_m and l_b are proportional to the pendulum arm length, we can conclude that decreasing the this length increases the recovery angle.

Moreover, we arrive to the same conclusion by analyzing the dynamic behavior of the system given by equation (1) by ignoring the effects of gravity and friction we get:

$$\ddot{\theta} = -\frac{\tau_c}{I_{so}} \tag{33}$$

which shows that the motor will produce greater acceleration $\ddot{\theta}$ for the same torque if the inertia I_{so} is lower.

Given that

$$I_{so} = I_{bo} + I_{ro} + I_{mo} =\propto M_b \cdot l_b^2 + M_R \cdot l_R^2 + M_m \cdot l_m^2$$

it can be sen that I_{so} is reduced by reducing the length of the pendulum arm.

UHMW (Ultra-high-molecular-weight polyethylene) was used as the material for the pendulum arm given that equations (2) and (3) have a term that increases linearly with M_b, meaning that a light material is needed. These predictions match the results found in simulation shown in Fig. 5.

This means that there is no optimal value for the pendulum height and it has to be chosen arbitrarily. We chose 30 degrees as the recovery angle of our system, which from Fig. 5 corresponds to a 207 mm long pendulum arm.

B. Reaction Wheel Design

The reaction wheel influences the dynamics of the system with its mass M_R as it can be seen in equation (1), and its inertia I_R as it can be seen in equation (6).

The design of the reaction wheel should aim to reduce the mass M_R as it decreases k_{mgl} and I_{so} because both have a term proportional to M_R. Section V-A shows that decreasing these parameters increases the recovery angle of the system.

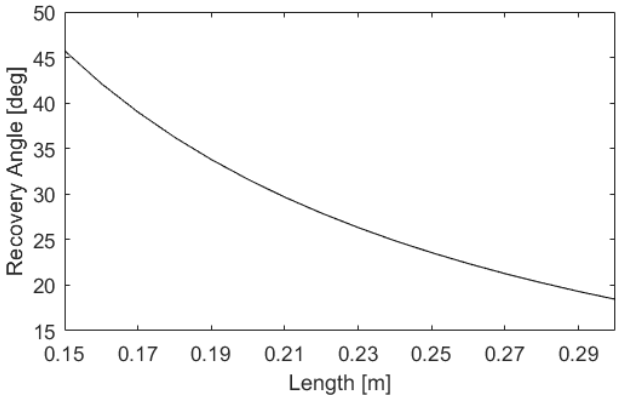

Fig. 5. Recovery angle plot of a system with varying length.

The design of the reaction wheel should aim to increase the inertia I_R as it increases the time the motor imparts torque on the arm, increasing the recovery angle. This is because a greater inertia leads to less angular acceleration for the same torque and therefore the time constant for the motor to reach saturation is larger. This can be seen in equations (34a) and (34b), obtained by ignoring the inductance in the electromechanical equations of the motor.

$$\begin{cases} \dot{\omega} = \dfrac{\tau_c}{I_R} & \text{(34a)} \\ \tau_e = \dfrac{k_t}{R}u(t) - \dfrac{k_t k_e}{R}\omega & \text{(34b)} \end{cases}$$

The geometry of the reaction wheel consists of a shaft coupling at its center, three spokes and an outer rim. The geometry and dimensions of the coupling are defined by the motor shaft and the set screws. The spokes have a thickness b and a width aR (Fig. 6). To maximize system performance, these spokes should be as thin as possible. However, because it's easier to manufacture, depth b is chosen to match the thickness of the outer rim and spoke width aR should be chosen big enough so that it can withstand machining forces during milling without bending.

Finally we are left with dimensions R_r, b and t (Fig. 7) which can be chosen to maximize the system performance.

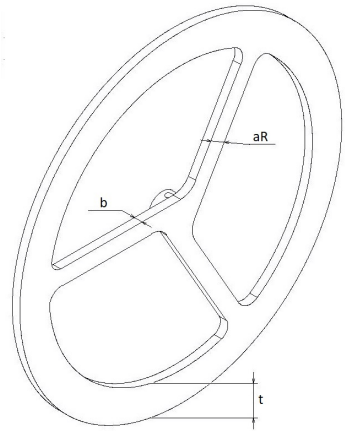

Fig. 6. Reaction wheel isometric view showing spokes dimensions.

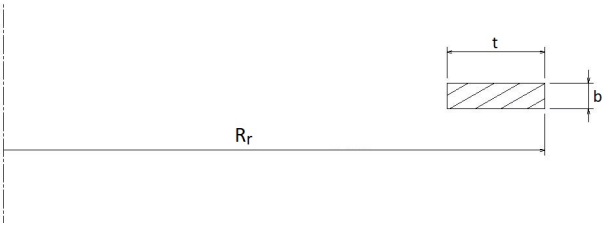

Fig. 7. Reaction wheel outer rim section view with general dimensions. Not including spokes.

1) Optimal Reaction wheel outer rim width t: To analyze how the recovery angle varies by changing t, we turn to simulation.

Fig. 8 shows how the recovery angle changes as we vary t while keeping all other parameters constant (motor characteristics, pendulum length, wheel thickness b, wheel radius).

It can be seen that there is an optimal value for the rim width t for this given set of parameters.

After performing the same analysis for different sets of parameters it was found that every set of parameters has an optimal value of t that maximizes the recovery angle. This is one of the most important results in this work because it renders one less independent value to analyze. In the analysis that follows, the optimal value for t will be calculated for every change in the other parameters. This can be done because the rim width has no manufacturability limitations.

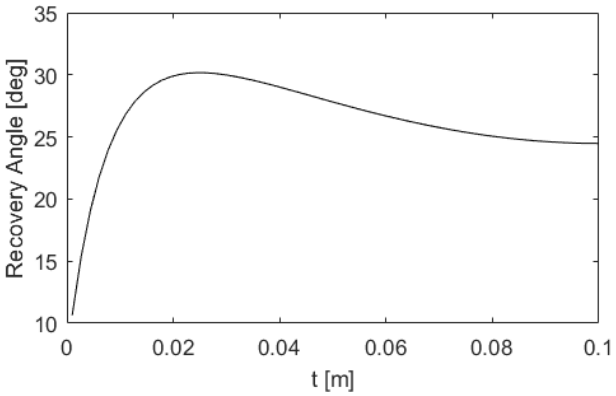

Fig. 8. Effect of varying t on the recovery angle.

2) Reaction wheel thickness b: To analyze the influence of this parameter, we perform a parameter sweep on the system for different values of b. Considering the result found in 1) that states that every set of parameters has an optimal value for t; we perform this parameter sweep by keeping almost all parameters constant except for t. For every value of b an optimal value of t is computed.

Fig. 9 and 10 show the results of this set of simulations. For this given pendulum, there is an optimal value of b at $8mm$ with a recovery angle of 31 degrees.

It should be noted on Fig. 9 that the sensitivity of the recovery angle to b near the optimal value is very small (recovery angle greater than 30 degrees for b values from $4.7mm$ to $15.4mm$), meaning that b can differ from the optimal value to satisfy other constraints without producing

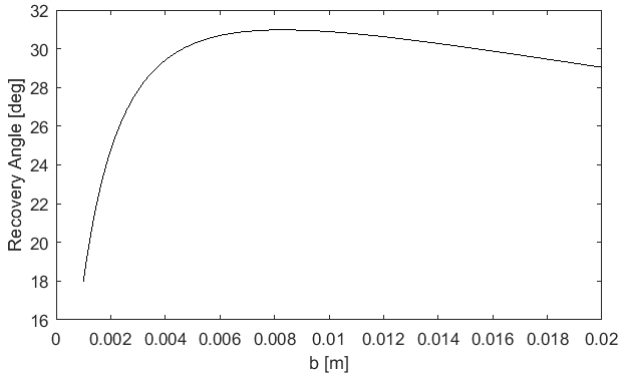

Fig. 9. Effect of varying b on the recovery angle.

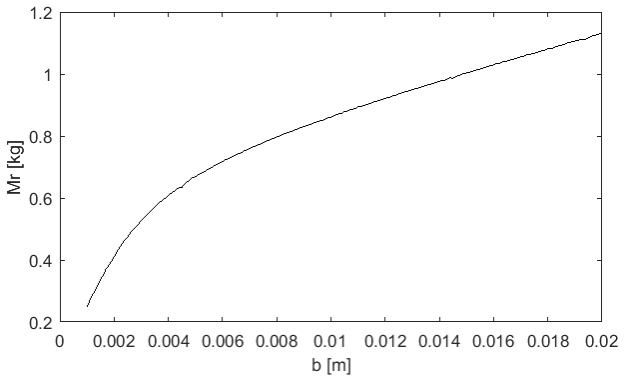

Fig. 10. Effect of varying b on the optimal reaction wheel mass.

a great reduction in the recovery angle. This is convenient because a reaction wheel with smaller b requires less raw materials, is easier to manufacture and is lighter (Fig. 10). For this reason $b = 5mm$ was chosen.

3) Reaction wheel radius R_r: Increasing R_r leads to an increase in the recovery angle of the system. This can be seen in Fig. 11, which was obtained by iterating over different systems varying R_r and optimizing t for each iteration.

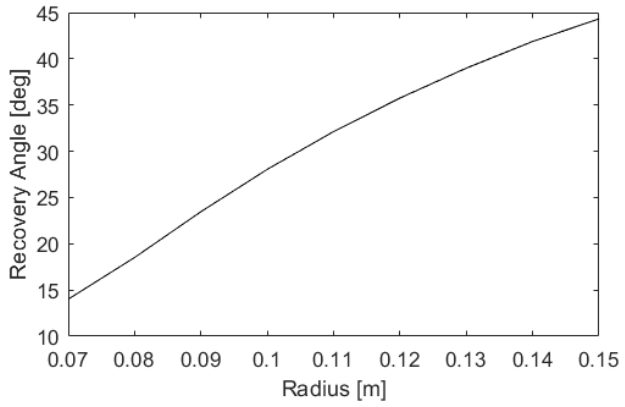

Fig. 11. Recovery angles for systems of increasing wheel radius and optimal rim width t in each case.

This behavior is expected because the wheel inertia I_r is proportional to M_r and approximately proportional to R_r^2, this makes it possible to increase the wheel inertia while decreasing its mass, which increases recovery angle.

For this project we selected $R_r = 105mm$ which is the biggest radius that could be machined with the available lathe.

4) Reaction wheel material density: To analyze the effect of this variable, we can vary ρ from $500\frac{kg}{m^3}$ to $20000\frac{kg}{m^3}$ which covers almost all the possible material densities available.This parameter sweep was performed by keeping almost all parameters constant and varying ρ while calculating the optimal value for t for every given ρ.

These results can be seen in Fig. 12 which shows a steep increase in recovery angle for ρ from $1000\frac{kg}{m^3}$ to about $8000\frac{kg}{m^3}$, meaning that materials such as plastics with a density of about $900\frac{kg}{m^3}$ and aluminum with $2700\frac{kg}{m^3}$ are not good choices compared to steel with a density of $7870\frac{kg}{m^3}$.

However, for materials denser than steel there is not a big increase in angle and, for even denser materials, the recovery angle decreases.

For these reasons, steel was chosen as the reaction wheel material.

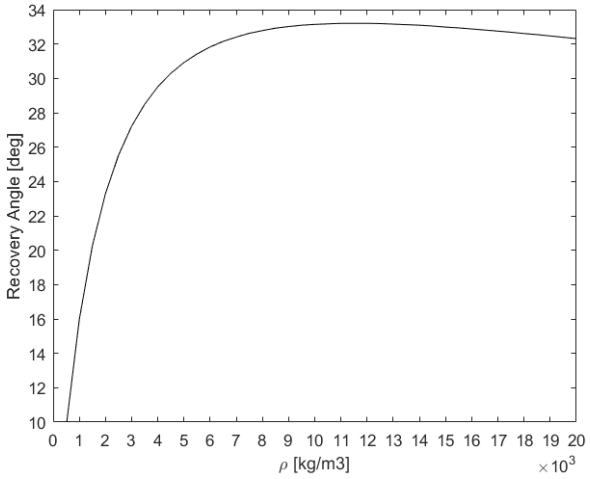

Fig. 12. Recovery angles for varying ρ with optimal t for every given ρ.

VI. Motor Selection

The two main requirements for the electric motor are:

High Stall Torque which leads to higher recovery angle values as seen in equation (32). To achieve this, high k_t and low R is needed as shown in equation (35).

$$\tau_{max} = k_t \frac{u}{R} \tag{35}$$

High Maximum Angular Velocity which allows the motor to apply torque for a longer amount of time as shown in equations (34a) and (34b). To achieve this, low k_e is needed as seen in equation (36).

$$\omega_{max} = \frac{u}{k_e} \tag{36}$$

Note that k_t and k_e are modeled separately, even though they are theoretically equal. This is because their measured value is not equal due to effects like friction. However, they are still mutually proportional.

To summarize, the high stall torque requirement demands for a high motor constant while the high maximum angular velocity requires a low motor constant. This means that there is an optimal value that satisfies both conditions.

A. Gearbox Ratio Optimization

The motor constants can be changed by changing the gearbox ratio as shown in equation (37).

$$k_t = K \cdot k_{tm} \tag{37}$$
$$k_e = K \cdot k_{em} \tag{38}$$

Where k_{tm} and k_{em} are the motor constants of the electric motor without gearbox and K is the gearbox ratio.

After defining the pendulum length, reaction wheel radius and b, the gear ratio can be optimized by varying K and calculating the optimal t for every value of K.

Fig. 13 shows that there is an optimal value of k at 10.

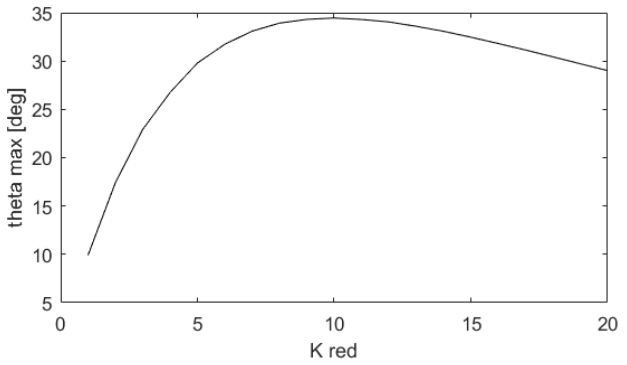

Fig. 13. Recovery angles for varying K with optimal t for every given K.

Due to availability, a gear ratio of 16 was chosen.

VII. Electrical Diagram of the System

Figure 14 shows a simplified diagram of the system. Two encoders where used to measure the states of the system. The system is plug and play and has its own power supply.

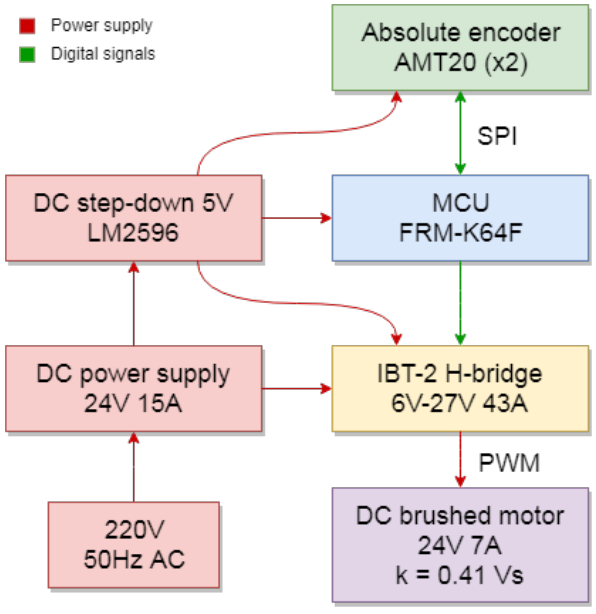

Fig. 14. Simplified electrical diagram of the system.

VIII. System Characterization

A. Mass and Moment of Inertia

Because the geometry of each part is known, the moment of inertia was calculated by just measuring their mass.

B. Motor Characterization

Subsection II-B enumerates all the characteristics of a direct current motor.

Resistance R and inductance L were measured by the use of an impedance measurement device while b_R and τ_{fd} were estimated by first calculating the total friction torque when the motor operating at 24V with zero load. On steady state, $\tau_c = 0$. From equation (8a) we get that:

$$\tau_{e0} = b_R \cdot \omega_{R0} + \tau_{fd} \tag{39}$$

τ_{e0} is estimated by measuring the total power the motor is using, subtracting the joule heating losses and calculating the torque for the its angular velocity

$$\tau_{e0} = \frac{u_0 i_0 - i_0^2 R}{\omega_{R0}} \tag{40}$$

by connecting 24V to the motor, accelerating the reaction wheel to its maximum speed and then disconnecting the power supply (high impedance), both friction components can be estimated. The following equation describes this experiment:

$$I_R \cdot \dot{\omega}_{Inertial} + b_R \cdot \omega_R + \tau_{fd} = 0 \tag{41}$$

Fig. 15 shows the results of this experiment. The values of b_R and τ_{fd} can be estimated as $b_R = 7.74 \times 10^{-4} Nms$ and $\tau_{fd} = 0.067 Nm$ by fitting equation (41) to the measured data using equation (39) as a constraint.

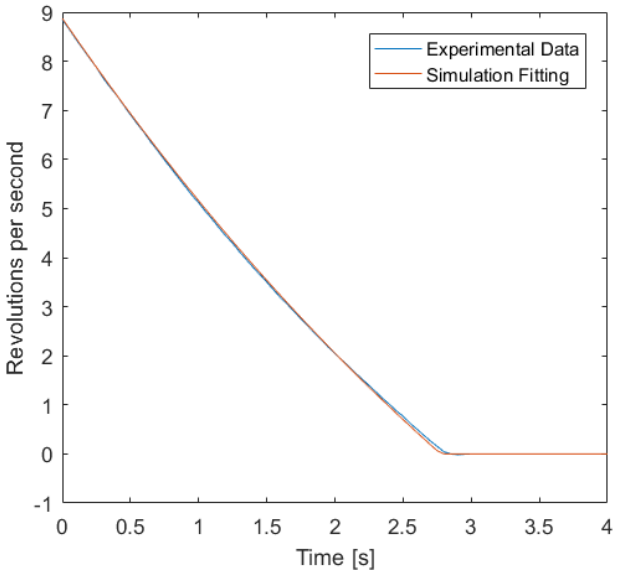

Fig. 15. Decelerating reaction wheel from maximum speed at 24V switched to high impedance at t=0 sec.

Motor constants k_e and k_t can be estimated as $k_e = 0.398 Vs$ and $k_t = 0.23 \frac{Nm}{A}$ by fitting the experimental curve obtained by applying a voltage step from 0V to 24V. This experiment is described by equations (6), (8a), (9a) ,(9b) and by taking $\dot{\theta} = 0$ in equation (7).

Fig. 16 shows the experimental and simulated response to a 24V step.

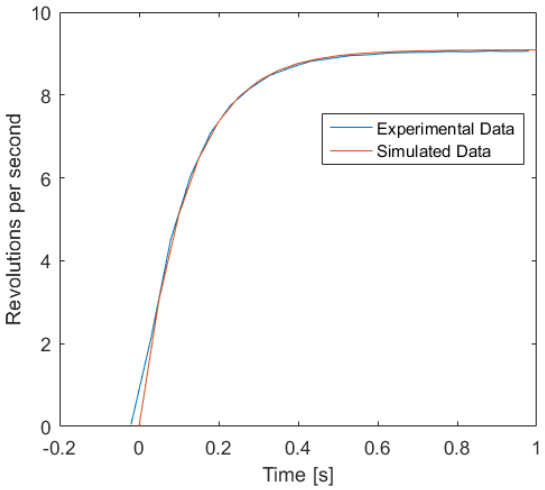

Fig. 16. Accelerating reaction wheel from maximum speed at 24V switched to high impedance at t=0 sec.

IX. Control System Design

A discrete time full state feedback control is used given that all states of the system can be measured directly.

The poles of the continuous linear state space model of the system (Eq (25), (26), (27) and (28)) are located at $1.07Hz$, $-0.94Hz$ and $-1.58Hz$.

The sampling frequency is selected as 10 times the frequency of the fastest pole of the open loop system, resulting in f = 20Hz. After selecting the sampling frequency, a discrete time description of the plant can be obtained as follows [7]:

$$x[k+1] = Gx[k] + Hu(k) \tag{42}$$

Where

$$G = \begin{bmatrix} 1.06 & 0.051 & 0.0009 \\ 2.41 & 1.06 & 0.0353 \\ -1.98 & -0.0526 & 0.6327 \end{bmatrix} \tag{43}$$

$$H = \begin{bmatrix} -0.0023 \\ -0.0868 \\ 0.9028 \end{bmatrix} \tag{44}$$

$$u(k) = K_1\theta(k) + K_2\dot{\theta}(k) + K_3\omega_R(k) \tag{45}$$

The z-plane poles of the discretized system are located at 1.4015, 0.7432 and 0.6081.

The feedback constants are calculated using a LQR that minimizes the cost function:

$$J = \sum_{n=1}^{\infty}[x^T(k)Qx(k) + u^T(k)Ru(k)] \tag{46}$$

The following weight matrices successfully stabilize the system:

$$Q = \begin{bmatrix} 1 & 0 & 0 \\ 0 & 1 & 0 \\ 0 & 0 & 1 \end{bmatrix} \tag{47}$$

$$R = 1 \tag{48}$$

Varying these weights does affect the system response to disturbances, steady state oscillations and control effort.

Further tuning of the LQR control could be carried out to improve transient behavior and robustness. However, this work focuses on optimizing the recovery angle which is designed under a saturated actuator, making it independent of the control system. Given that only stabilization was sought, the tuning of the LQR Q and R matrices is considered to be out of the scope of this work.

The controller was implemented with the following state feedback constants:

$$K_1 = -124, K_2 = -18.6, K_3 = -0.957 \tag{49}$$

X. Real System Performance

To analyze the correspondence between the real system and the simulated model, a recovery experiment was performed by placing the pendulum at a 25° angle and turning the control system on.

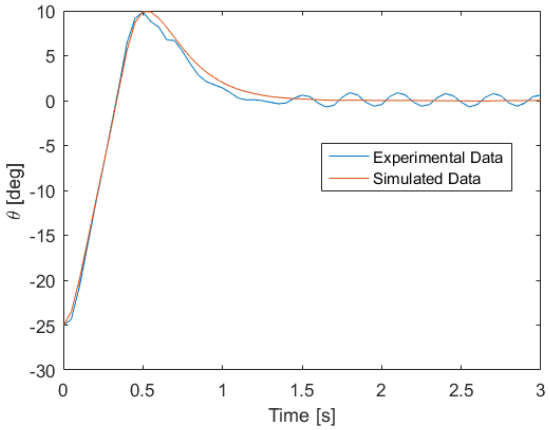

Fig. 17. Simulation and Real system recovering from an initial angle of 25°.

Fig 17 shows the result of the experiment. It can be seen that the real response is very close to the simulated response. The main difference is on steady state, where the real system presents an oscillation due to static friction on the electric motor.

The predicted recovery angle from simulation also matches the real recovery angle. Figures 19 and 18 show two recovery experiments from 26.1° and 26.7° respectively and their corresponding simulations. The real and simulated systems were able to stabilize starting from 26.1° but they were not able to stabilize from 26.7°, meaning that the exact recovery angle is between these two values, and that simulation predicted the real recovery angle within less than 0.6°.

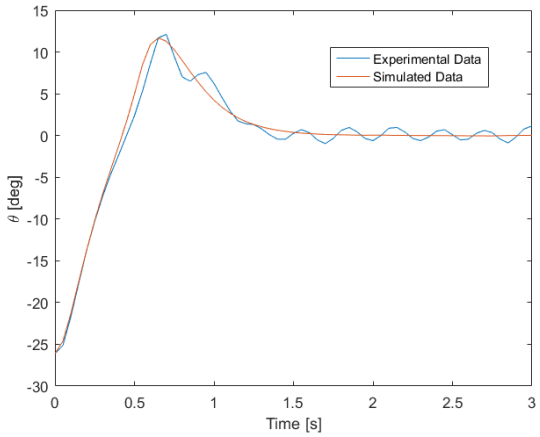

Fig. 18. Recovery experiment from 26.1°. The pendulum was able to stabilize from this angle.

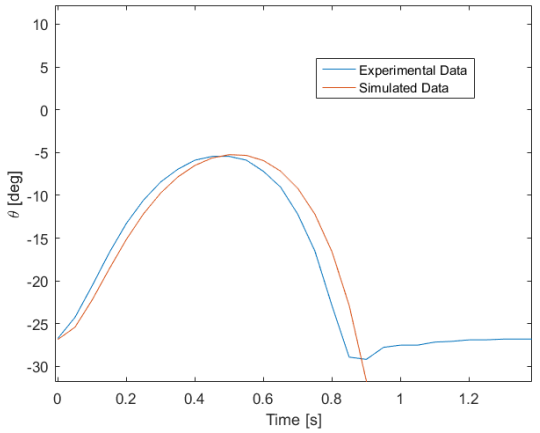

Fig. 19. Recovery experiment from 26.7°. The pendulum was not able to stabilize from this angle.

XI. Conclusion

The reaction wheel inverted pendulum system can be optimized to maximize recovery angle and system performance. This paper identifies the parameters that do or do not influence the system performance, and describes several design criteria for these parameters. Both the reaction wheel rim width and the gearbox ratio have specific values that maximize system performance for any given system. Some other parameters should be increased or decreased to maximize system performance until some other constraint is reached.

Experiments show that the model of the system corresponds to the real behavior, meaning that conclusions drawn from simulations are valid in the real system.

Acknowledgment

We would like to thank Dr. Ghersin for guiding and inspiring us to present this work at ARGENCON 2018, Dr. Nemirovsky for his guidance on this work and Dr. Aguirre for enabling us to keep working on this project by providing financing.

References

[1] M. Gajamohan, M. Merz, I. Thommen, and R. D'Andrea, "The cubli: A cube that can jump up and balance," in *2012 IEEE/RSJ International Conference on Intelligent Robots and Systems*, Oct 2012, pp. 3722–3727.

[2] B. R. Andrievsky, "Global stabilization of the unstable reaction-wheel pendulum," *Automation and Remote Control*, vol. 72, no. 9, p. 1981, Sep 2011. [Online]. Available: https://doi.org/10.1134/S0005117911090189

[3] D. M. Alonso, E. E. Paolini, and J. L. Moiola, "Controlling an inverted pendulum with bounded controls," in *Dynamics, Bifurcations, and Control*, F. Colonius and L. Grüne, Eds. Berlin, Heidelberg: Springer Berlin Heidelberg, 2002, pp. 3–16.

[4] J. Meyer, N. Delson, and R. A. de Callafon, "Design, modeling and stabilization of a moment exchange based inverted pendulum," *IFAC Proceedings Volumes*, vol. 42, no. 10, pp. 462 – 467, 2009, 15th IFAC Symposium on System Identification. [Online]. Available: http://www.sciencedirect.com/science/article/pii/S1474667016386906

[5] G. Belascuen. Reaction wheel balanced inverted pendulum. [Online]. Available: https://www.youtube.com/watch?v=nFSflKQajQU

[6] Mathworks matlab simulink (r2016a). [Online]. Available: http://www.mathworks.com/products/simulink/

[7] K. Ogata, *Discrete Time Control Systems*, 2nd ed. Englewood Cliffs, NJ: Prentice-Hall International, Inc., 1995.